Millimeter-Wave MIMO-NOMA based Positioning System for Internet of Things Applications

Millimeter-Wave MIMO-NOMA based Positioning System for Internet of Things Applications

Lincong Han, Rongke Liu, *Senior Member, IEEE,* Zijie Wang, Xinwei Yue, *Member, IEEE* and John S. Thompson, *Fellow, IEEE*

***Abstract*—Non-orthogonal multiple access (NOMA) has been identified as a promising technology in millimeter-wave (mmWave) multiple-input multiple-output (MIMO) communication networks for Internet of things (IoT) applications, which has the advantages of both massive connectivity and high spectrum efficiency. However, few researchers have considered the probability of introducing NOMA to a positioning system. In this paper, a novel mmWave MIMO-NOMA based positioning system is proposed, which is capable of meeting the requirements of IoT applications. We establish a NOMA-based positioning model from the perspective of the system level, along with the design of transmission strategy. To characterize the positioning performance, the position error bound (PEB) is selected as an evaluation criteria and theoretical expressions of the PEB are provided. Simulations of comparing localization performance between NOMA and conventional orthogonal multiple access (OMA) are conducted by using the theoretical analysis. Numerical results show that the application of NOMA to localization is a viable way to reduce the PEB compared to OMA. Our work further shows under what circumstances can NOMA outperform OMA in terms of localization performance and the corresponding parameter settings.**

***Index Terms*—Internet of things, millimeter wave, MIMO, non-orthogonal multiple access, position error bound**

I. Introduction

The Internet of things (IoT) is deemed as a revolutionary paradigm of communication which builds a bridge from the physical world towards the cyber world to realize the interconnection, interaction and intelligent decision of everyday objects [1]. According to related surveys, the number of IoT devices has been growing unprecedentedly and will reach 100 billion by 2025 [2]. These IoT devices include sensors, actuators, autonomous vehicles, etc., and they can be applied in industrial environments, urban infrastructures, and so forth [3]. There are multiple factors that make the emergence of IoT become a revolution of the communication paradigm [4], among which is communication. Many specific promising techniques have been designed to satisfy the requirements of communications, which include high mobility, massive connectivity, low latency, etc., such as millimeter-wave (mmWave), multiple-input multiple-output (MIMO) and non-orthogonal multiple access (NOMA) [5].

MmWave communication operating in 30-300 GHz is utilized to increase the spectrum range of current networks [6]. For IoT applications, mmWave is proved to alleviate the traffic pressure drastically [7]. The authors in [8] show that mmWave is the only viable solution for vehicle-to-vehicle communication. MIMO is proposed to improve channel capacity and spectrum efficiency, which can be usefully applied to IoT networks [9]. NOMA can help save physical blocks (frequency channels and time slots) in IoT communication [10]. Applying NOMA in machine-to-machine systems, the authors of [11] show the improvement of throughput efficiency. The authors in [12] utilize NOMA to IoT to achieve diverse QoS. The application of NOMA to mmWave IoT system has been discussed in [13].

Since a majority of IoT applications are location-based services [14], localization plays an important role in IoT communication. The relationship between communication and localization can be regarded as a synergistic interaction because channel estimation provides angle of arrival (AOA) or angle of departure (AOD) can be used as indirect information for localization. In turn, location information helps the transmitter to better design beamforming strategies. At this moment, can communication techniques such as mmWave, MIMO and NOMA be applied to positioning system? Actually, these three techniques have been regarded as potential methods for positioning. And currently, there have been a lot of researches on the performance analysis and estimation algorithms in mmWave MIMO positioning systems.

From the perspective of location, the higher temporal diversity obtained by mmWave is capable of improving the estimation accuracy of positioning parameters greatly, i.e., time difference of arrival and AOA [15]. The authors in [16] figure out that the positioning accuracy of received signal strength indicator (RSSI) in 60 GHz indoor networks can reach one meter. In a mmWave scenario, where BS is equipped with multiple antennas while the UE has a single antenna, positioning error bound (PEB) is analyzed, and three estimator named Maximum Likelihood (ML) 2D, Unstructured ML and method-of-moment are adopted to estimate AOD and time of flight (TOF) in [17]. Moreover, the authors of [18] consider the trade-off between communication and positioning in single-user mmWave communication by balancing the effective data

This work was supported by the Beijing Municipal Science and Technology Project (Z181100003218008). (*Corresponding author: Rongke Liu.)*

L. Han, R. Liu, and Z. Wang are with School of Electronic and Information Engineering, Beihang University, Beijing100191, China (email: {lincong_han, rongke_liu, wangmajie}@buaa.edu.cn).

X. Yue is with School of Information Communication and Engineering, Beijing Information Science Technology University, Beijing100101, China (email: xinwei.yue@bistu.edu.cn).

J. S. Thompson is with the Institute for Digital Communications, School of Engineering, University of Edinburgh, King's Buildings, Edinburgh, EH9 3JL, U.K. (e-mail: john.thompson@ed.ac.uk).

rate (communication parameter) and position-rotation error bound (positioning parameter).

MIMO positioning is nowadays a popular topic because it provides high angle resolution, which results in more accurate estimation of AOA and AOD. Furthermore, MIMO positioning exceeds other positioning techniques such as global positioning system (GPS), Wi-Fi, bluetooth etc., in that it does not need external technologies to interface with mobile system [19]. In [20], the authors propose a novel positioning method for massive MIMO that based on AOA and time of arrival estimates, and show the framework which can enable the detection and estimation. The authors in [21] draw their attention to the wideband massive antenna array positioning performance and calculate the error bound of such system. The result of localization can be utilized to enhance massive MIMO communication quality by avoiding pilot contamination, which is proposed in [22].

There also exist many researches on positioning system which combine mmWave and MIMO. In [23, 24], the authors provide the positioning error bounds and estimation algorithm of orientation in 5G mmWave MIMO systems. Unlike the research mentioned above, the authors of [25, 26] paid attention to the positioning error bounds (PEBs) of mmWave 3-D MIMO for both uplink and downlink communications. Moreover, a beamspace channel model for sparse mmWave MIMO system is built up and the corresponding localization algorithm is proposed which is based on the channel sparsity masks in [27].

To the best of our knowledge, NOMA has hardly been utilized to positioning for localization, although it has potential value when the trade-off between communication and localization needs to be considered, as is shown in [28]. The authors in [28] design a multi-scale NOMA-MIMO system and analyze the basic positioning and communication performance, where positioning signals are superimposed with data signals. However, this work does not take the possibility of superimposing different users' positioning signals into account. Moreover, to solve the problem of the heavy pilot overhead caused by the increase of the user numbers, NOMA has been considered. Related work on non-orthogonal pilots superposition is shown in [29], which designs some possible patterns of pilot superposition. But the paper only analyzes the capacity and data rates, not the localization performance. Therefore, state of art, there has not been research on the design and performance analysis of positioning signals' non-orthogonal superposition.

As a result, although mmWave, MIMO and NOMA are beneficial to positioning, their combination in IoT scenarios is still an open issue, since the application of NOMA to mmWave MIMO positioning system has remained absent so far.

A. Motivations and Contributions

We have determined that the application of NOMA to mmWave-MIMO IoT positioning system has potential value. Here, we use the scenario where heterogenous positioning and the trade-off between communication and positioning are required as an example. As is shown in Fig. 1, assuming that there are two IoT devices waiting to be served. Device 1 is willing to be localized more accurate than Device 2, so that its positioning signal is longer than Device 2's. While data transmission requirement is not that important. When applying OMA, the BS transmits their signals one by one, according to the time order, that is, the BS first transmits Device 1's pilot signal, along with its data signal. Then, Device 2's pilot signal and data signal are transmitted sequentially. If we constrain the length of a frame, then adopt NOMA, the pilot signals are non-orthogonally superimposed, and the remaining space of one frame is reserved for data transmission. To compensate for the power loss caused by the superposition, the pilot signals can be lengthened. Under this circumstance, the total time allocated to these two devices' pilot signals is reduced, thus increasing the capacity of the data transmission phase. So, distributing non-orthogonal positioning signals to different devices will have advantages on improving the QoS or the overall system performance under some situations where multiple BSs localizing one device, heterogeneous requirements of positioning or the trade-off between communication and localization needs to be considered.

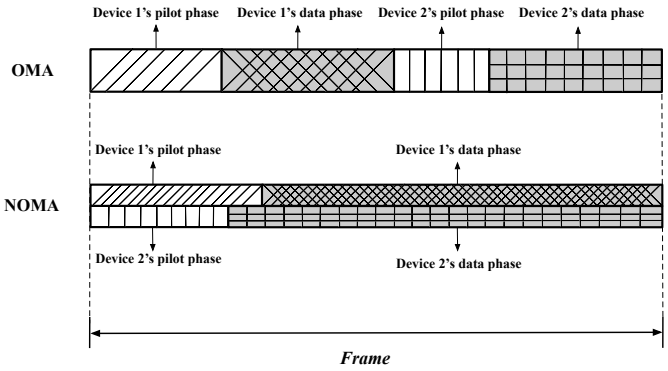

Fig. 1: In an IoT scenario, Device 1 has higher positioning requirement than Device 2, and the total length of one frame is constrained. When adopting OMA, signals are transmitted chronologically. While for NOMA, pilots are non-orthogonally superimposed and transmitted simultaneously.

In our paper, the application of NOMA to mmWave-MIMO localization system is investigated in detail. Different powers are assigned to multiple IoT devices' pilots and allow them to be transmitted in the same frequency band. At the receiver, successive interference cancellation (SIC) is employed to distinguish these positioning signals. The positioning performance is characterized in terms of PEB. We first consider a two-device scenario, where the PEBs of a pair of devices (i.e., a nearby device and a distant device) are studied respectively, and then extend the system to a multiple-device scenario to give a more general form of the PEB. A two-stage method is utilized to derive the PEB. Firstly, the Fisher information matrix (FIM) of the channel parameters is calculated, such as time of arrival, AOD, and the channel complex gain. Then, the FIM of the channel parameters is transformed into the FIM of location parameters by a bijection matrix transformation. Finally, the PEB can be obtained by inverting the FIM and calculating the trace. The main contributions of this paper can be summarized as follows:

- We establish the mmWave MIMO-NOMA based localization system for the first time. We introduce NOMA to conventional mmWave MIMO system to improve the localization performance. Besides, we specify a transmission strategy based on the user pairing method to make our system more realistic. The power allocation method is also used in numerical simulation.
- Our work provides the PEBs of mmWave MIMO-NOMA localization system for the first time both by theoretical derivation and numerical simulation in a two-device scenario. We show that the adoption of NOMA to localization can obtain double the number of positioning data compared to OMA, which can improve the accuracy of localization under the assumption of being given the same amount of resources (spectrum, time slots etc.). Besides, we also reveal the theoretical expressions of FIM in multiple-device scenario, which represents a general form of PEB in this system.
- For practical application purpose, we give guidance on what total transmission power and power allocation ratio should be set at the BS to embody the advantages of NOMA versus OMA. Besides, the influence of devices' distances to BS are also analyzed and can be in turn serve as recommendation for practical use.

B. Organization and Notations

The rest of this paper is organized as follows. The system model of mmWave MIMO-NOMA based positioning system is introduced in Section II. Theoretical analysis of PEB are derived in Section III. Section IV reveals the numerical results of PEB in mmWave MIMO-NOMA system and the comparison between NOMA and OMA. Finally, the conclusions are drawn in Section V.

We use the following notations throughout the paper: $\mathbf{A}$ is a matrix, $\mathbf{a}$ is a vector, and a is a scalar. $\|\mathbf{A}\|_{\mathrm{F}}$ is the Frobenius norm of $\mathbf{A}$, whereas $\mathbf{A}^{\mathrm{T}}$, $\mathbf{A}^{\mathrm{H}}$, $\mathbf{A}^{-1}$ is its transpose conjugate transpose and inverse, respectively. Besides, $\mathbb{E}[\cdot]$ denotes the expectation operation and $\Re\{\cdot\}$ means the real-part operator.

II. System Model

In this section, the system model of mmWave MIMO-NOMA based localization is established carefully, which is designed for IoT applications. Furthermore, we present the transmission strategy and transmission model.

A. System Design

As shown in Fig. 2, we consider an IoT scenario where one BS serves multiple IoT devices such as intelligent robots and monitors, smart meters, logistic devices and autonomous cars, etc., so that their requirements of positioning is diverse, which is reflected on the difference of positioning signals for different devices. The BS employs a uniform linear array of N_{BS} antennas and adopts mmWave downlink multi-user MIMO when communicating with IoT devices, while each IoT device has a single antenna because of the limitation of size and power.

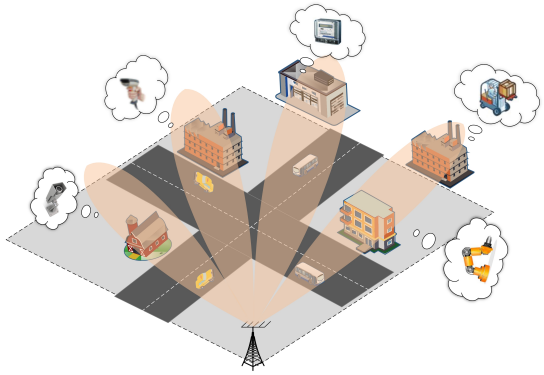

Fig. 2: In an IoT scenario, BS is equipped with N_{BS} antennas and adopts mmWave downlink networks. IoT devices located in the same beam can adopt NOMA, and each of them is single-antenna.

Power domain cluster-based NOMA is adopted for transmission [30], and the transmission strategy is shown in Fig. 3. Assuming that there are K IoT devices within one beam. At the BS side, the user pairing method is that IoT devices within the same beam geographically are seen as a group. Their signals are firstly distributed with different power levels (K levels in total) according to their channel conditions, and then superposed as a composite signal to be transmitted in the same frequency. At the receiver side, each device first decodes other devices' signals with larger power and utilizes SIC to remove them, and then decodes its own signal.

B. Signal Model

The signal waveform for NOMA is based on orthogonal frequency division multiplexing, which is aimed at utilizing its advantages of frequency reuse and MIMO affinity [31]. Assuming that the mmWave carrier frequency is f_c (corresponding to wavelength λ_c) and bandwidth is B. There are G composite signals transmitted sequentially, and the number of subcarriers is N. In the g-th transmission for the n-th subcarrier, the k-th device's signal containing M symbols can be expressed as:

$$\boldsymbol{x}_k^g[n] = [x_{k,1}[n] \ \cdots \ x_{k,M}[n]]^{\mathrm{T}}, \tag{1}$$

where $g = 0, \ldots, G-1$, $n = 0, \ldots, N-1$ and $k = 1, 2, \ldots K$. Then the composite signal can be expressed as:

$$\boldsymbol{x}^g[n] = \sum_{k=1}^{K} \sqrt{a_k P}\boldsymbol{x}_k^g[n], \tag{2}$$

where P is the total transmission power and a_k is the power allocation ratio of the k-th device, which satisfies the condition $\sum_{k=1}^{K} a_k = 1$.

In this paper, we adopt hybrid precoding, for its advantages of significantly improving achievable rate in mmWave MIMO communication [32]. Besides, there are two specific hybrid precoding that can be selected according to their advantages: fully-connected and sub-connected hybrid precoding. The fully-connected hybrid precoding method is

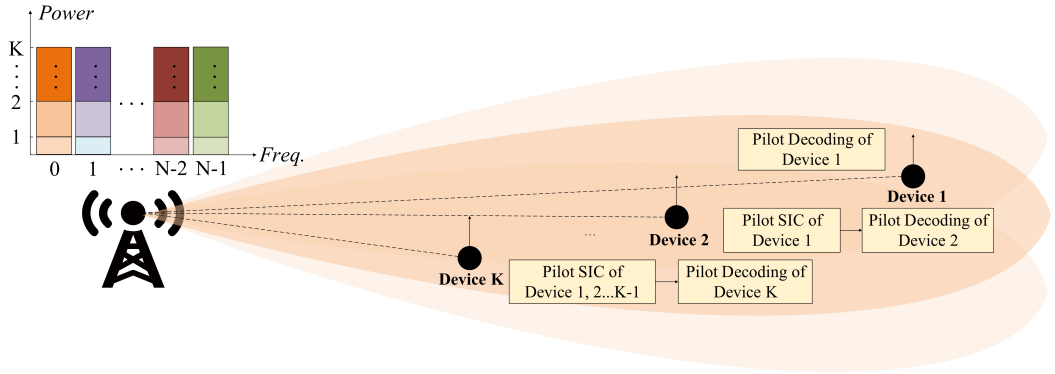

Fig. 3: In mmWave MIMO-NOMA system, within one beam, total power is divided into K levels and distributed to K devices' signals. These signals are superimposed non-orthogonally before transmission. Receivers decode their own signals by adopting SIC, except that the farthest one decodes its signal directly.

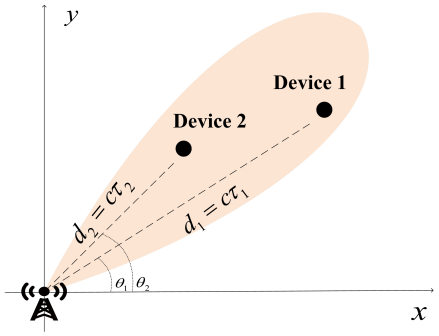

Fig. 4: The LOS links between BS and devices are considered in this positioning problem, where the location of BS is known. Devices' position, as well as AOD θ_k, distance d_k, delay τ_k and the channel gain are to be estimated.

applied to reduce the number of RF chains (N_{RF}) [33]. While sub-connected architecture can improve energy efficiency [34]. The beamforming matrix is denoted as $\mathbf{F}^g[n] = \mathbf{F}^g_{RF}\mathbf{F}^g_{BB}[n] \in \mathbb{C}^{N_{BS}\times M}$, where $\mathbf{F}^g_{RF} \in \mathbb{C}^{N_{BS}\times N_{RF}}$ and $\mathbf{F}^g_{BB}[n] \in \mathbb{C}^{N_{RF}\times M}$ are the high-dimensional analog and low-dimensional digital precoding matrix, respectively. We normalize that $\|\mathbf{F}^g[n]\|_{\mathrm{F}} = 1$. For directional beamforming, we have $\mathbf{F}^g[n] = \frac{1}{\sqrt{M}}[\boldsymbol{f}_1,\ \boldsymbol{f}_2,\ \ldots \boldsymbol{f}_M]$, where

$$\boldsymbol{f}_m = \frac{1}{\sqrt{N_{BS}}}\left[1,\ e^{j\frac{2\pi}{\lambda}d\psi_m},\ \ldots e^{j(N_{BS}-1)\frac{2\pi}{\lambda}d\psi_m}\right]^{\mathrm{T}}, \quad (3)$$

and $\psi_m = \vartheta + \frac{2(m-1)}{M}$ is the phase of the m-th beam and ϑ denotes an initial phase randomly following a uniform distribution between -1 and 1 [35].

Based on the above assumptions, the received signal of the k-th device for the n-th subcarrier and the g-th transmission after Fast Fourier Transform can be given by:

$$y^g_k[n] = \boldsymbol{h}^{\mathrm{T}}_k[n]\mathbf{F}^g[n]\boldsymbol{x}^g[n] + w^g[n], \quad (4)$$

where $\boldsymbol{h}^{\mathrm{T}}_k[n]$ denotes the channel vector from BS to the k-th device in the n-th carrier, and $w^g[n]$ is the addictive complex Gaussian noise with zero mean and variance σ^2. Then the transmission signal-noise-ratio (SNR) can be expressed as $\gamma \triangleq \frac{P}{\sigma^2}$.

The set of all the received signals of the k-th device, $\mathbf{Y}_k$, can be directly obtained:

$$\mathbf{Y}_k = \begin{bmatrix} y^1_k[0] & \cdots & y^G_k[0] \\ \vdots & \ddots & \vdots \\ y^1_k[N-1] & \cdots & y^G_k[N-1] \end{bmatrix}, \quad (5)$$

where $k = 1, 2, \ldots K$.

C. Channel Model

In this paper, we consider the line-of-sight (LOS) mmWave communication, where the received power of diffuse scattering is much lower than that in NLOS [13]. According to [23], the channel vector from BS to the k-th device in the n-th carrier can be expressed as

$$\boldsymbol{h}^{\mathrm{T}}_k[n] = \sqrt{N_{BS}}\alpha_k e^{\frac{-j2\pi n\tau_k}{NT_s}}\mathbf{a}^{\mathrm{H}}_{BS}(\theta_k), \quad (6)$$

where $T_S = 1/B$ denotes the sampling duration and $\alpha_k = h/\sqrt{\rho_k}$ denotes the equivalent channel complex gain, which combines the identical complex channel gain for all devices h and the k-th device's path loss ρ_k. The equivalent channel gain α_k can also be expressed as $\alpha_k = r_k \exp(j\phi_k)$, with r_k and ϕ_k its amplitude and phase. The propagation duration $\tau_k = d_k/c$, with d_k the distance between BS and the k-th device. Besides, $\mathbf{a}_{BS}(\theta_k) \in \mathbb{C}^{N_{BS}\times 1}$ is the k-th device's antenna steering vector, with θ_k the AOD from the BS to the k-th device. Notice that when $B \ll f_c$, the wavelength of the n-th subcarrier $\lambda_n = \frac{c}{f_c + n/(NT_s)} \approx \lambda_c$. The steering vector is given by

$$\mathbf{a}_{BS}(\theta) = \left[1, e^{j\frac{2\pi}{\lambda_c}d\sin\theta}, \ldots, e^{j(N_{BS}-1)\frac{2\pi}{\lambda_c}d\sin\theta}\right]^{\mathrm{T}}. \quad (7)$$

The two dimensional illustration of the system model (two-device case) can be seen in Fig. 4, where the BS is located at the origin and $\boldsymbol{p}_k = [p_{k,x}, p_{k,y}]^{\mathrm{T}} \in \mathbb{R}^2$ is the unknown position of the k-th device ($k = 1, \ldots, K$). We have introduced the distance between antenna elements $d = \lambda_c/2$

to (7). Without loss of generality, channels are sorted as $\|\boldsymbol{h}_1\|^2 \leq \|\boldsymbol{h}_2\|^2 \leq \cdots \leq \|\boldsymbol{h}_K\|^2$ and $a_1 \geq a_2 \geq \cdots \geq a_K$.

III. POSITIONING PERFORMANCE EVALUATION

In this section, the positioning performance of mmWave MIMO-NOMA system is investigated in terms of PEB in both two-device and multiple-device scenarios. For illustration purposes, we first derive the FIM of the nearby device and distant device under a two-device case and further consider the multiple-device scenario. Then the Cramér-Rao bound is analyzed by using the FIM.

In NOMA process, the nearby device has better channel condition but less transmission power than distant device, which applies SIC to remove distant device's signal after receiving the compound signal from BS. It is assumed that the nearby device adopts perfect SIC and the interference only comes from the environment noise[1]. While the distant device can not eliminate the nearby device's influence and take it as interference. Under such assumption, the noise-free observation of the i-th ($i = 1, 2$) device's signal at the j-th ($j = 1, 2$) device's side for the n-th subcarrier and g-th transmission can be expressed as

$$m_{ij}^{g}[n] = \sqrt{a_i P N_{BS}}\alpha_j \exp(\frac{-j2\pi n\tau_j}{NT_s})\mathbf{a}_{BS}^{\mathrm{H}}(\theta_j)\, \boldsymbol{s}_i^{g}[n], \quad (8)$$

where $\boldsymbol{s}_k^{g}[n] = \mathbf{F}^{g}[n]\boldsymbol{x}_k^{g}[n]$. The power allocation ratios of distant and nearby device are denoted by a_1 and a_2, respectively, with the relationship of $a_1 > a_2$ and $a_1 + a_2 = 1$.

To obtain the FIM of the devices' position, the FIM of channel parameters is derived first. Let $\boldsymbol{\eta}_k$ be the unknown parameter vector of the k-th device's channel, and be written as:

$$\boldsymbol{\eta}_k = [r_k\ \phi_k\ \tau_k\ \theta_k]^{\mathrm{T}}. \quad (9)$$

Assuming that $\hat{\boldsymbol{\eta}}_k$ is the unbiased estimator of $\boldsymbol{\eta}_k$, then the mean squared estimation (MSE) bound is expressed as

$$\mathbb{E}_{\boldsymbol{Y}_k|\boldsymbol{\eta}_k}\left[(\hat{\boldsymbol{\eta}}_k - \boldsymbol{\eta}_k)(\hat{\boldsymbol{\eta}}_k - \boldsymbol{\eta}_k)^{\mathrm{T}}\right] \geq \mathbf{J}_{\boldsymbol{\eta}_k}^{-1}, \quad (10)$$

where $\mathbb{E}_{\boldsymbol{Y}_k|\boldsymbol{\eta}_k}[\cdot]$ denotes the conditional expectation operation and $\mathbf{J}_{\boldsymbol{\eta}_k}$ is the 4×4 FIM of the k-th device defined as [37]

$$\begin{aligned}\boldsymbol{J}_{\boldsymbol{\eta}_k} &= \mathbb{E}_{\boldsymbol{Y}_k|\eta_k}\left[-\frac{\partial^2 \ln f(\boldsymbol{Y}_k|\boldsymbol{\eta}_k)}{\partial\boldsymbol{\eta}_k\partial\boldsymbol{\eta}_k^{\mathrm{T}}}\right] \\ &= \sum_{n=0}^{N-1}\sum_{g=1}^{G}\mathbb{E}_{y_k|\boldsymbol{\eta}_k}\left[-\frac{\partial^2 \ln f(y_k|\boldsymbol{\eta}_k)}{\partial\boldsymbol{\eta}_k\partial\boldsymbol{\eta}_k^{\mathrm{T}}}\right],\end{aligned} \quad (11)$$

where $f(y_k|\boldsymbol{\eta}_k)$ denotes the conditional likelihood function of y_k under the condition of known $\boldsymbol{\eta}_k$.

In the following parts we will further derive the specific expressions of (11) for different kinds of devices.

[1]The impact of imperfect SIC [36] to positioning performance will be taken into account in our future work.

A. Nearby Device's FIM of Channel Parameters

For nearby device, as is proved in [37], the conditional likelihood function is

$$f(y_2|\boldsymbol{\eta}_2) \propto \exp\left\{\frac{1}{\sigma^2}m_{22}^{\mathrm{H}}[n]y_2[n] - \frac{1}{2\sigma^2}\|m_{22}[n]\|^2\right\}, \quad (12)$$

where $\propto$ denotes equality up to irrelevant constants. Then we obtain

$$\mathbb{E}_{y_2|\boldsymbol{\eta}_2}\left[-\frac{\partial^2 \ln f(y_2|\boldsymbol{\eta}_2)}{\partial\boldsymbol{\eta}_2\partial\boldsymbol{\eta}_2^{\mathrm{T}}}\right] = \begin{bmatrix}\Phi_2(r_2,r_2) & \Phi_2(r_2,\phi_2) & \Phi_2(r_2,\tau_2) & \Phi_2(r_2,\theta_2)\\ \Phi_2(\phi_2,r_2) & \Phi_2(\phi_2,\phi_2) & \Phi_2(\phi_2,\tau_2) & \Phi_2(\phi_2,\theta_2)\\ \Phi_2(\tau_2,r_2) & \Phi_2(\tau_2,\phi_2) & \Phi_2(\tau_2,\tau_2) & \Phi_2(\tau_2,\theta_2)\\ \Phi_2(\theta_2,r_2) & \Phi_2(\theta_2,\phi_2) & \Phi_2(\theta_2,\tau_2) & \Phi_2(\theta_2,\theta_2)\end{bmatrix}, \quad (13)$$

with

$$\Phi_2(x_1,x_2) = \frac{1}{\sigma^2}\Re\left\{\frac{\partial m_{22}^{\mathrm{H}}[n]}{\partial x_1}\frac{\partial m_{22}[n]}{\partial x_2^{\mathrm{T}}}\right\}. \quad (14)$$

Applying (8) to (14), the elements' expressions of nearby device's MSE (shown in (13)) can be obtained:

$$\Phi_2(r_2,r_2) = \Re\left\{\xi_2\mathbf{a}_{2,n}^{\mathrm{H}}(\theta_2)\mathbf{X}_{2,0}\mathbf{a}_{2,n}(\theta_2)\right\}, \quad (15)$$

$$\Phi_2(r_2,\phi_2) = \Re\left\{jr_2\xi_2\mathbf{a}_{2,n}^{\mathrm{H}}(\theta_2)\mathbf{X}_{2,0}\mathbf{a}_{2,n}(\theta_2)\right\}, \quad (16)$$

$$\Phi_2(r_2,\tau_2) = \Re\left\{-jr_2\xi_2\mathbf{a}_{2,n}^{\mathrm{H}}(\theta_2)\mathbf{X}_{2,1}\mathbf{a}_{2,n}(\theta_2)\right\}, \quad (17)$$

$$\Phi_2(r_2,\theta_2) = \Re\left\{-j\pi r_2\xi_2\cos\theta_2\mathbf{a}_{2,n}^{\mathrm{H}}(\theta_2)\mathbf{X}_{2,0}\mathrm{a}_{2,D,n}(\theta_2)\right\}, \quad (18)$$

$$\Phi_2(\phi_2,\phi_2) = \Re\left\{\xi_2 r_2^2\mathbf{a}_{2,n}^{\mathrm{H}}(\theta_2)\mathbf{X}_{2,0}\mathbf{a}_{2,n}(\theta_2)\right\}, \quad (19)$$

$$\Phi_2(\phi_2,\tau_2) = \Re\left\{-r_2^2\xi_2\mathbf{a}_{2,n}^{\mathrm{H}}(\theta_2)\mathbf{X}_{2,1}\mathbf{a}_{2,n}(\theta_2)\right\}, \quad (20)$$

$$\Phi_2(\phi_2,\theta_2) = \Re\left\{-\pi r_2^2\xi_2\cos\theta_2\mathbf{a}_{2,n}^{\mathrm{H}}(\theta_2)\mathbf{X}_{2,0}\mathbf{a}_{2,D,n}(\theta_2)\right\}, \quad (21)$$

$$\Phi_2(\tau_2,\tau_2) = \Re\left\{r_2^2\xi_2\mathbf{a}_{2,n}^{\mathrm{H}}(\theta_2)\mathbf{X}_{2,2}\mathbf{a}_{2,n}(\theta_2)\right\}, \quad (22)$$

$$\Phi_2(\tau_2,\theta_2) = \Re\left\{\pi r_2^2\xi_2\cos\theta_2\mathbf{a}_{2,n}^{\mathrm{H}}(\theta_2)\mathbf{X}_{2,1}\mathbf{a}_{2,D,n}(\theta_2)\right\}, \quad (23)$$

$$\Phi_2(\theta_2,\theta_2) = \Re\left\{\pi^2 r_2^2\xi_2\cos^2\theta_2\mathbf{a}_{2,D,n}^{\mathrm{H}}(\theta_2)\mathbf{X}_{2,0}\mathbf{a}_{2,D,n}(\theta_2)\right\}, \quad (24)$$

where $\mathbf{D} = \underset{l}{\mathrm{diag}}[0\ 1\ \cdots(N_{BS}-1)]$, $\xi_2 = a_2\gamma N_{BS}$, $\mathbf{X}_{2,l} = \left(\frac{2\pi n}{NT_s}\right)^l\boldsymbol{x}_2[n]\boldsymbol{x}_2^{\mathrm{H}}[n]$, $\mathbf{a}_{2,n}(\theta_2) = (\mathbf{F}^{g}[n])^{\mathrm{H}}\mathbf{a}_{BS}(\theta_2)$, $\mathbf{a}_{2,D,n}(\theta_2) = (\mathbf{F}^{g}[n])^{\mathrm{H}}\mathbf{D}\mathbf{a}_{BS}(\theta_2)$.

Besides, it is easy to notice that matrix $\mathbf{J}_{\eta_2}$ is a conjugate symmetric matrix, so the rest elements of $\mathbf{J}_{\eta_2}$ can be easily obtained by conjugation operation. Finally, the specific elements of (12) can be obtained.

B. Distant Device's FIM of Channel Parameters

For distant device, as mentioned above, it regards nearby device's signal as noise, so the total noise can be expressed as

$$z_1[n] = m_{21}[n] + w[n], \tag{25}$$

from which we can directly figure out that the noise $z_1[n]$ still meets Gaussian distribution. The power of nearby device's signal which distant device receives can be expressed as

$$\begin{aligned}\|m_{21}[n]\|^2 &= \left\| \sqrt{a_2 P N_{BS}} r e^{j\phi} \exp(\frac{-j2\pi n\tau}{NT_s}) \mathbf{a}_1^{\mathrm{H}}(\theta_1) \mathbf{F} \right\|^2 \\ &= \frac{a_2 P r^2}{M N_{BS}} \sum_{m=1}^{M} \sum_{h=0}^{N_{BS}-1} \sum_{i=0}^{N_{BS}-1} e^{j\pi(h-i)(\psi_m - \sin\theta_1)},\end{aligned} \tag{26}$$

where σ_1^2 denotes the variance of $z_1[n]$ and can be easily obtained

$$\sigma_1^2 = \sigma^2 + \frac{a_2 P r^2}{M N_{BS}} \sum_{m=1}^{M} \sum_{h=0}^{N_{BS}-1} \sum_{i=0}^{N_{BS}-1} e^{j\pi(h-i)(\psi_m - \sin\theta_1)}. \tag{27}$$

Under these circumstances, the conditional likelihood function of y_1 changes into the following form [37]

$$f(y_1|\boldsymbol{\eta}_1) = \frac{1}{\sqrt{2\pi\sigma_1^2}} \exp\left\{ -\frac{(y_1[n] - m_{11}[n])^2}{2\sigma_1^2} \right\}. \tag{28}$$

As a further development, FIM of channel parameters can be expressed as

$$\begin{aligned}&\mathbf{J}_{\boldsymbol{\eta}_1} = \\ &\sum_{n=0}^{N-1} \sum_{g=1}^{G} \Re\left\{ \frac{1}{\sigma_1^2} \frac{\partial m_{11}^{\mathrm{H}}[n]}{\partial \boldsymbol{\eta}_1} \frac{\partial m_{11}[n]}{\partial \boldsymbol{\eta}_1^T} + \frac{1}{2}\left(\frac{1}{\sigma_1^2}\right)^2 \frac{\partial \sigma_1^2}{\partial \boldsymbol{\eta}_1} \frac{\partial \sigma_1^2}{\partial \boldsymbol{\eta}_1^{\mathrm{T}}} \right\}.\end{aligned} \tag{29}$$

The first term of (29) can be directly obtained by replacing the subscript 1 by 2 of (13) and then multiply $\frac{1}{\sigma_1^2}$. For the second term, we have

$$\frac{\partial \sigma_1^2}{\partial r_1} = \frac{2 a_2 P r_1}{M N_{BS}} \sum_{m=1}^{M} \sum_{h=0}^{N_{BS}-1} \sum_{i=0}^{N_{BS}-1} e^{j\pi(h-i)(\psi_m - \sin\theta_1)}, \tag{30}$$

$$\frac{\partial \sigma_1^2}{\partial \phi_1} = \frac{\partial \sigma_1^2}{\partial \tau_1} = 0, \tag{31}$$

$$\begin{aligned}&\frac{\partial \sigma_1^2}{\partial \theta_1} = \\ &\frac{a_2 P r_1^2}{M N_{BS}} \sum_{m=1}^{M} \sum_{h=0}^{N_{BS}-1} \sum_{i=0}^{N_{BS}-1} j\pi(i-k)\cos\theta_1 e^{j\pi(h-i)(\psi_m - \sin\theta_1)}.\end{aligned} \tag{32}$$

So

$$\frac{\partial \sigma_1^2}{\partial \boldsymbol{\eta}_1} \frac{\partial \sigma_1^2}{\partial \boldsymbol{\eta}_1^T} = \begin{bmatrix} \left(\frac{\partial \sigma_1^2}{\partial r_1}\right)^2 & 0 & 0 & \frac{\partial \sigma_1^2}{\partial \theta_1}\frac{\partial \sigma_1^2}{\partial r_1} \\ 0 & 0 & 0 & 0 \\ 0 & 0 & 0 & 0 \\ \frac{\partial \sigma_1^2}{\partial r_1}\frac{\partial \sigma_1^2}{\partial \theta_1} & 0 & 0 & \left(\frac{\partial \sigma_1^2}{\partial \theta_1}\right)^2 \end{bmatrix}. \tag{33}$$

C. Multiple NOMA Devices' FIM of Channel Parameters

In this part, there are more than two devices conducting NOMA operation is considered in detail.

First, we focus attention on the K-th device, which has the best channel condition and will directly decode its signal without the use of SIC. Thus, $\mathbf{J}_{\boldsymbol{\eta}_K}$ will be similar as (13)

$$\begin{aligned}&\mathbb{E}_{y_K|\boldsymbol{\eta}_K}\left[-\frac{\partial^2 \ln f(y_K|\boldsymbol{\eta}_K)}{\partial \boldsymbol{\eta}_K \partial \boldsymbol{\eta}_K^{\mathrm{T}}} \right] = \\ &\begin{bmatrix} \Phi_K(r_K, r_K) & \Phi_K(r_K, \phi_K) & \Phi_K(r_K, \tau_K) & \Phi_K(r_K, \theta_K) \\ \Phi_K(\phi_K, r_K) & \Phi_2(\phi_K, \phi_K) & \Phi_K(\phi_K, \tau_K) & \Phi_K(\phi_K, \theta_K) \\ \Phi_K(\tau_K, r_K) & \Phi_K(\tau_K, \phi_K) & \Phi_K(\tau_K, \tau_K) & \Phi_K(\tau_K, \theta_K) \\ \Phi_K(\theta_K, r_K) & \Phi_K(\theta_K, \phi_K) & \Phi_K(\theta_K, \tau_K) & \Phi_K(\theta_K, \theta_K) \end{bmatrix},\end{aligned} \tag{34}$$

with

$$\Phi_K(x_1, x_2) = \frac{1}{\sigma^2} \Re\left\{ \frac{\partial m_{KK}^{\mathrm{H}}[n]}{\partial x_1} \frac{\partial m_{KK}[n]}{\partial x_2^{\mathrm{T}}} \right\}. \tag{35}$$

For the k-th device, when adopting SIC, it can detect the l-th ($1 \le k$) device's signal and perfectly eliminate it, while the rest devices' signals are regarded as noises. In this way, the variance of total noise σ_k^2 is

$$\sigma_k^2 = \sigma^2 + \left\| \sum_{l=k+1}^{K} m_{lk}[n] \right\|^2. \tag{36}$$

With similar processing, FIM concerning channel parameters of the k-th device $\mathbf{J}_{\boldsymbol{\eta}_k}$ can be derived, which is not repeated here.

D. PEB Calculation

This section is to obtain the expression of FIM of device's position parameters, and show the calculation method for PEB. It is noticed that we omit the subscript in this part because the following procedures are totally the same for all devices. The device's position parameters can be expressed as follows:

$$\tilde{\boldsymbol{\eta}} = [r \ \phi \ p_x \ p_y]^{\mathrm{T}}. \tag{37}$$

By means of a bijective transformation, the FIM of $\tilde{\boldsymbol{\eta}}$, i.e $\mathbf{J}_{\tilde{\boldsymbol{\eta}}}$, can be obtained from $\mathbf{J}_{\boldsymbol{\eta}}$, that is

$$\mathbf{J}_{\tilde{\boldsymbol{\eta}}} = \mathbf{T} \mathbf{J}_{\boldsymbol{\eta}} \mathbf{T}^{\mathrm{H}}, \tag{38}$$

where

$$\mathbf{T} = \frac{\partial \boldsymbol{\eta}^{\mathrm{T}}}{\partial \tilde{\boldsymbol{\eta}}} = \begin{bmatrix} \frac{\partial r}{\partial r} & \frac{\partial \phi}{\partial r} & \frac{\partial \tau}{\partial r} & \frac{\partial \theta}{\partial r} \\ \frac{\partial r}{\partial \phi} & \frac{\partial \phi}{\partial \phi} & \frac{\partial \tau}{\partial \phi} & \frac{\partial \theta}{\partial \phi} \\ \frac{\partial r}{\partial p_x} & \frac{\partial \phi}{\partial p_x} & \frac{\partial \tau}{\partial p_x} & \frac{\partial \theta}{\partial p_x} \\ \frac{\partial r}{\partial p_y} & \frac{\partial \phi}{\partial p_y} & \frac{\partial \tau}{\partial p_y} & \frac{\partial \theta}{\partial p_y} \end{bmatrix}. \tag{39}$$

After simple calculation, the elements of $\mathbf{T}$ are shown below:

$$\partial r/\partial r = \partial \phi/\partial \phi = 1,$$

$$\frac{\partial \tau}{\partial p_x} = \frac{p_x}{c\sqrt{p_x^2 + p_y^2}}, \quad \frac{\partial \tau}{\partial p_y} = \frac{p_y}{c\sqrt{p_x^2 + p_y^2}},$$

TABLE I: PEB RESULTS VERSUS NOMA DEVICES' LOCATION

PEB [m]	within the 1st Beam ($d_k = 30$m, k $= 1, 2$)	Maximum Value	Minimum Value	Range
Nearby Device	0.5378	2.1514	0.0276	2.1238
Distant Device	0.4468	1.0565	0.1713	0.8852

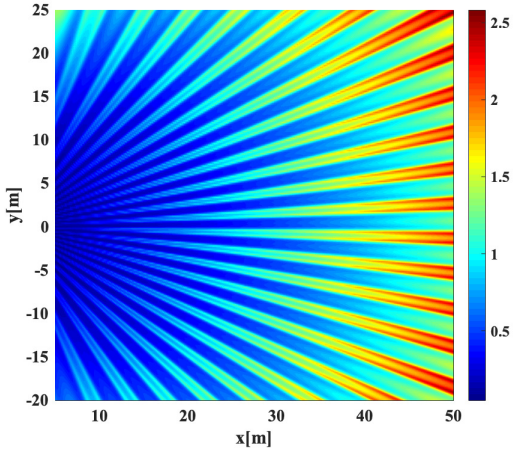

Fig. 5: PEB for NOMA nearby device in a 50 m $\times 50$ m square with SNR ranges 25 dB when $a_1 = 0.6,\ a_2 = 0.4$.

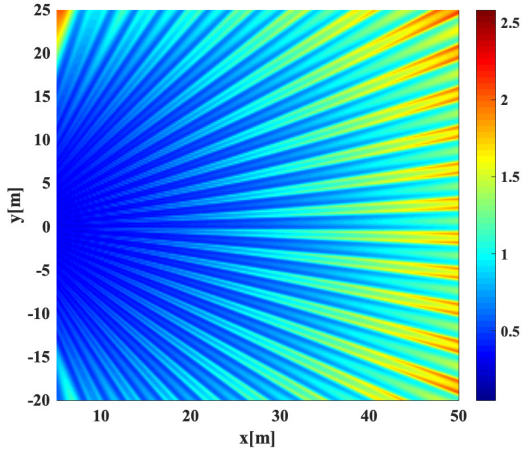

Fig. 6: PEB for NOMA distant device in a 50 m $\times 50$ m square with SNR ranges 25 dB when $a_1 = 0.6,\ a_2 = 0.4$.

$$\frac{\partial \theta}{\partial p_x} = \frac{-p_y}{p_x^2 + p_y^2}, \quad \frac{\partial \theta}{\partial p_y} = \frac{p_x}{p_x^2 + p_y^2},$$

with the rest elements zero. The PEB then can be expressed as

$$\text{PEB} = \sqrt{\left[\mathbf{J}_{\tilde{\boldsymbol{\eta}}}^{-1}\right]_{3,3} + \left[\mathbf{J}_{\tilde{\boldsymbol{\eta}}}^{-1}\right]_{4,4}}, \tag{40}$$

where $\left[\mathbf{J}_{\tilde{\boldsymbol{\eta}}}^{-1}\right]_{j,j}$ means selecting the j-th element of the diagonal line of $\mathbf{J}_{\tilde{\boldsymbol{\eta}}}$'s inverse matrix.

IV. SIMULATION RESULTS

In this section, we show the PEB of NOMA devices in different positions, and compare the positioning performance between NOMA and OMA to figure out their advantages and disadvantages in different transmission conditions. The simulation is carried out in a square area with side length 50 m. The number of antennas for BS is set to be 65. The beam number is set to be 25 to obtain a better coverage of target devices' localization, as is demonstrated in [23, 26], which is also in line with the non-singular condition conformed in [24, 38]. For mmWave transmission, the carrier frequency f_c is set to be 60 GHz, with bandwidth $B = 100$ MHz [39]. Besides, the speed of light c is 0.3 m/ns. In the following simulation, we set $G = 1$, $N = 20$ to satisfy the non-singular condition proved in [17], that is, at least one of the parameter G and N should be larger than 1. The channel model $h = (1 + j)/\sqrt{2}$. We adopt the geometry based statistical path loss model mentioned in [40, 41], where the path loss ρ_k is decided by free space path loss $\text{FSPL}(d_k)$ and atmosphere attenuation $\mu^2(d_k)$. According to the measurement result in [38], atmosphere attenuation coefficient is 16 dB/Km. Using this model, the path loss of the k-th user can be expressed as

$$\rho_k = \mu^2(d_k) \cdot \text{FSPL}(d_k), \tag{41}$$

where $\text{FSPL}(d_k) = \left(\frac{4\pi d_k}{\lambda_c}\right)^2$.

Abundant positioning performance evaluation results using different kinds of multiple access methods, NOMA and OMA will be presented. For the purpose of fair comparison, we assume a two-device case and there are two resource blocks (RBs). In OMA, devices need to be transmitted one by one, which means one RB can only serve one device, while in NOMA, two devices can be served simultaneously in one RB. So by using two resource blocks, each OMA device can only acquire one set of position measurement, while each NOMA device can get two position measurements, which makes full use of NOMA's advantages, that is, high resource utilization. Besides, to make sure that the two devices are within the same beam, through the simulation, we set the same AODs for nearby and distant device. Based on these results, some insights will be given as guidance for engineering applications.

Fig. 5 and Fig. 6 plot the PEB of two NOMA devices versus devices' positions. We set the power allocation ratio to be 0.4 for nearby device and 0.6 for distant device, and the total SNR ranges 25dB. Besides, we evade the origin to get more realistic result[2]. We can learn from the two figures that the PEB of both nearby and distant devices are much smaller within beams compared to the places out of beams. What is more, the PEB increases as devices get farther from the BS, which

[2]The positioning performance around the origin will be distorted, and there will be singularity that is misleading for us to analyze the PEB of other positions in this square area.

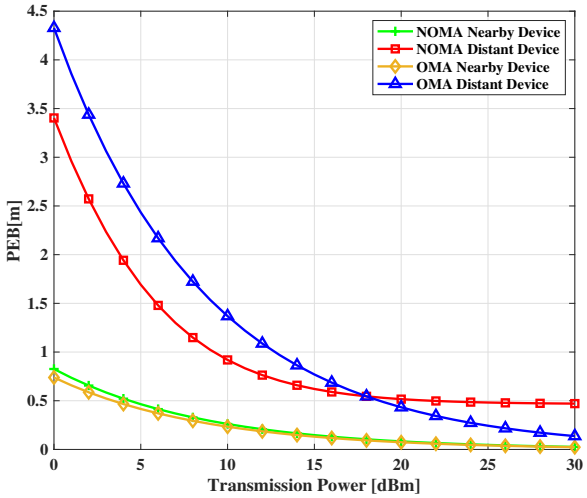

Fig. 7: PEB comparison between NOMA and OMA with total transmission power ranging from 0 to 30 dBm when $d_1 = 50$ m, $d_2 = 20$ m and $a_1 = 0.6$, $a_2 = 0.4$.

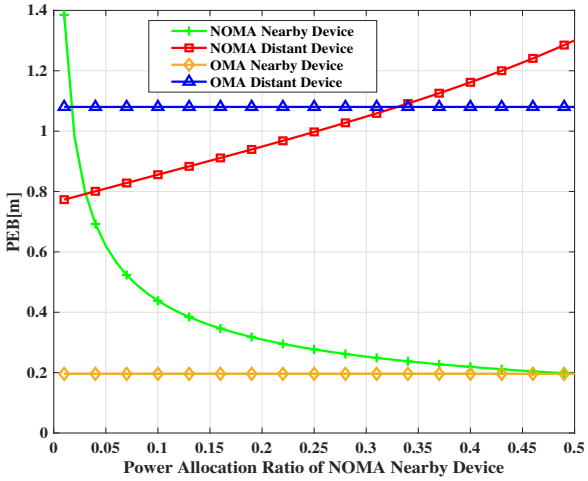

Fig. 8: PEB comparison between NOMA and OMA with power allocation ratio of NOMA nearby device ranging from 0 to 0.5 when $d_1 = 50$ m, $d_2 = 20$ m and total transmission power is 10 dBm.

is because the increase of path loss leads to the total SNR's decrease. As can be observed from Fig. 5 and Fig. 6, the PEB within beams when the distance between devices and BS is 30 m, maximum PEB, minimum PEB, and PEB range of nearby device and distant device are shown in TABLE. I. It shows that within the beam, when NOMA distant device and nearby device are in the same place, NOMA distant device has better positioning performance than nearby device. It can be explained by the larger power allocation ratio distributed to distant device. Moreover, through the square area, nearby device has the smallest and largest PEB value in comparison with distant device, which is due to their difference in the method of processing the composite signal: The interference introduced by nearby device's positioning signal is not much different compared to distant device, so that the change of path loss through different distance from BS to distant device is not significant compared to the strength of nearby device's positioning signal.

After traversing the PEB in the square area, we further investigate three factors that influence the PEB of NOMA and OMA IoT devices: total transmission power, power allocation ratio and distance from BS, and make comparison between them. Fig. 7 plots the PEB comparison between OMA and NOMA devices against the total transmission power. We fix the power allocation ratio to $a_1 = 0.6$, $a_2 = 0.4$ and the distance of OMA/NOMA's distant devices are 50 m while their nearby devices are 20 m far away from the BS. It is shown that nearby device's positioning accuracy is sacrificed because of the lower power allocation, but the difference between nearby OMA and NOMA device decreases with the increase of transmission power. However, for distant device, the NOMA device's PEB can be lower than OMA when transmission power is lower than around 18 dBm. For instance, when transmission power is 0 dBm, the NOMA distant device's PEB is 3.40 m while OMA distant device's PEB is 4.33 m, which means adopting NOMA can reduce the PEB by around 21.48%. It can be explained that when channel condition is not satisfied, the interference of the NOMA nearby device's signal can be neglected because it is much weaker than noise, while the nearby device's stronger power allocation coefficient and source thrift show their advantages. For the fact that in mmWave transmission, the path loss can be severe and SNR can be extremely lower than 0 dB, our research may provide a new method to improve the positioning accuracy.

Fig. 8 shows the PEB comparison between OMA and NOMA devices against power allocation coefficients. The total transmission power is set as 10 dBm, and the distance of nearby device and distant device are 20 m and 50 m, respectively. We traverse NOMA nearby device's power allocation ratio a_2 from 0.01 to 0.5, so that the power ratio of NOMA distant device is $a_1 = 1 - a_2$. It is shown that for distant device, applying NOMA can always outperform OMA if power is distributed to it more than 67%. At the same time, the more power it obtains, the lower PEB the NOMA distant device can reach in comparison with OMA distant device of the same distance. For instance, when $a_1 = 0.99$, $a_2 = 0.01$, PEB of OMA and NOMA distant device are 1.08 m and 0.77 m respectively, with the PEB difference 0.31 m, which indicates that in this situation, the application of NOMA can reduce the PEB by 28.70%. The curve of NOMA distant device's PEB versus power allocation coefficient is steep, in that with the increase of nearby device's power allocation ratio, which means that for distant device, it is distributed with less power and suffers more interference from nearby device. These two negative influences make its PEB increase quickly. When the ratio is approximated to 0.5, the power of nearby device's signal is almost the same with distant device's signal power. So, the interference coming from the nearby signal reaches the biggest level and the PEB is maximum. What we should also pay attention to is the worse performance of nearby device

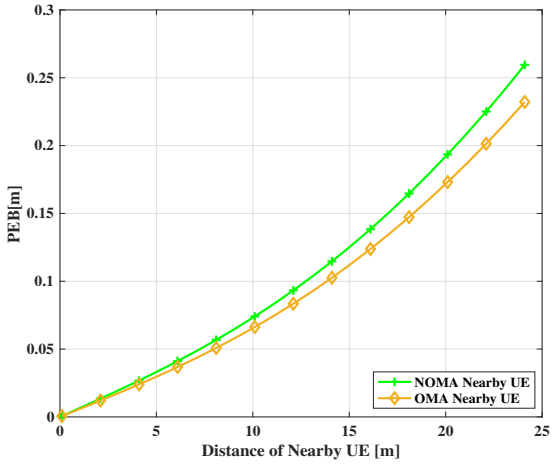

Fig. 9: PEB comparison between NOMA and OMA with distance of nearby device ranging from 0 to 25 m when $a_1 = 0.6,\ a_2 = 0.4$ and total transmission power is 10 dBm.

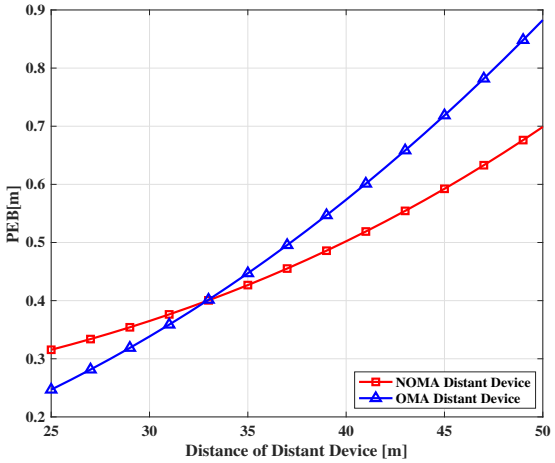

Fig. 10: PEB comparison between NOMA and OMA with distance of distant device ranging from 25 m to 50 m when $a_1 = 0.6,\ a_2 = 0.4$ and total transmission power is 10 dBm.

conducting NOMA compared to OMA. From (13) and (41), the NOMA nearby device's PEB is the power function of a_2 with power equals to -0.5, which is in accordance with Fig. 8. So for practical application, when adopting NOMA, in consideration of fairness, the power allocation coefficient should not be smaller than 0.33 for nearby device.

Fig. 9 and Fig. 10 show the PEB comparison between OMA and NOMA devices against distance to BS. Here we assume that power allocation coefficient is $a_1 = 0.6,\ a_2 = 0.4$ and the total transmission power is 10 dBm. Besides, nearby device's distance to BS is lower than 25 m while the distant device's distance ranges from 25 m to 50 m. From Fig. 9 we can learn that for the nearby device, applying NOMA indeed improves its PEB. However, the difference is really negligible compared to the PEB decrease distant device produces as is shown in Fig. 10. To specify, for the distant device, NOMA can outperform OMA when distance is farther than around 33 m, and PEB can be cut down by 0.18 m when the distant device's distance is 50 m. However, for the nearby device, the PEB difference is lower than 0.03 m. Combining Fig. 9 and Fig. 10, we can draw a conclusion that the larger the distance difference between the nearby and the distant device, the better NOMA performs than OMA.

V. Conclusion

In this paper, we introduce NOMA to mmWave MIMO IoT localization system and evaluate the performance compared with a conventional OMA system. The system design and transmission strategy are presented carefully. Theoretical analysis is accomplished to derive the PEBs of the distant and the nearby device in a two-device case respectively. Then the derivation is extended to multiple-device scenario. We compare the PEBs of the NOMA and the OMA devices respectively through numerical simulations on three parameters (total transmission power, power allocation ratio and devices' distance) to give benchmarks for future investigation of channel estimations. Numerical results demonstrate that NOMA can outperform OMA by up to 20% when the SNR is extremely low, which means that adopting NOMA is quite suitable in mmWave transmission. By power allocation, the distant device's PEB can be reduced by up to 28.70%. The larger the distance of the distant device, the better the effect of applying NOMA instead of OMA. Thus, applying NOMA to mmWave MIMO positioning system is able to improve the positioning performance, especially for those devices suffering bad channel condition, compared to OMA. We hope our work would provide meaningful inspiration for mmWave MIMO-NOMA positioning system for IoT application, especially in the situation where heterogenous positioning requirement, trade-off between communication and positioning or multiple BSs needs to be considered.

References

[1] L. D. Xu, W. He, and S. Li, "Internet of things in industries: A survey," *IEEE Trans. Ind. Inform.*, vol. 10, no. 4, pp. 2233–2243, Nov. 2014.

[2] K. Rose, S. Eldridge, and L. Chapin, "The Internet of Things: An Overview," in *Proc. Internet Soc. (ISOC)*, Reston, VA, USA, Oct. 2015, pp. 1–53.

[3] E. S. Lohan, M. Koivisto, O. Galinina, S. Andreev, A. Tolli, G. Destino, M. Costa, K. Leppanen, Y. Koucheryavy, and M. Valkama, "Benefits of positioning-aided communication technology in high-frequency industrial IoT," *IEEE Commun. Mag.*, vol. 56, no. 12, pp. 142–148, Dec. 2018.

[4] A. Al-Fuqaha, M. Guizani, M. Mohammadi, M. Aledhari, and M. Ayyash, "Internet of things: A survey on enabling technologies, protocols, and applications," *IEEE Commun. Surv. Tutor.*, vol. 17, no. 4, pp. 2347–2376, 4th Quart. 2015.

[5] A. Ali, W. Hamouda, and M. Uysal, "Next generation M2M cellular networks: challenges and practical considerations," *IEEE Commun. Mag.*, vol. 53, no. 9, pp. 18–24, Sep. 2015.

[6] M. R. Akdeniz, Y. Liu, M. K. Samimi, S. Shu, S. Rangan, T. S. Rappaport, and E. Erkip, "Millimeter wave channel modeling and cellular capacity evaluation," *IEEE J. Sel. Areas Commun.*, vol. 32, no. 6, pp. 1164–1179, Jun. 2014.

[7] Y. Chen, D. Chen, Y. Tian, and T. Jiang, "Spatial lobes division-based low complexity hybrid precoding and diversity combining for mmWave IoT systems," *IEEE Internet Things J.*, vol. 6, no. 2, pp. 3228–3239, Apr. 2019.
[8] J. Choi, V. Va, N. Gonzalez-Prelcic, R. Daniels, C. R. Bhat, and R. W. Heath, "Millimeter-wave vehicular communication to support massive automotive sensing," *IEEE Commun. Mag.*, vol. 54, no. 12, pp. 160–167, Dec. 2016.
[9] B. M. Lee and H. Yang, "Massive MIMO for industrial internet of things in cyber-physical systems," *IEEE Trans. Ind. Inform.*, vol. 14, no. 6, pp. 2641–2652, Jun. 2018.
[10] Y. Liu, Z. Qin, M. Elkashlan, Z. Ding, A. Nallanathan, and L. Hanzo, "Nonorthogonal Multiple Access for 5G and Beyond," *Proc. IEEE*, vol. 105, no. 12, pp. 2347–2381, Dec. 2017.
[11] M. Shirvanimoghaddam, M. Dohler, and S. J. Johnson, "Massive non-orthogonal multiple access for cellular IoT: Potentials and limitations," *IEEE Commun. Mag.*, vol. 55, no. 9, pp. 55–61, Sep. 2017.
[12] Z. Ding, L. Dai, and H. V. Poor, "MIMO-NOMA design for small packet transmission in the Internet of Things," *IEEE Access*, vol. 4, pp. 1393–1405, Aug. 2016.
[13] T. Lv, Y. Ma, Z. Jie, and P. T. Mathiopoulos, "Millimeter-wave NOMA transmission in cellular M2M communications for Internet of Things," *IEEE Internet Things J.*, vol. 5, no. 3, pp. 1989–2000, Jun. 2018.
[14] R. C. Shit, S. Sharma, D. Puthal, and A. Y. Zomaya, "Location of Things (LoT): A review and taxonomy of sensors localization in IoT infrastructure," *IEEE Commun. Surv. Tutor.*, vol. 20, no. 3, pp. 2028–2061, 3rd Quart. 2018.
[15] H. El-Sayed, G. Athanasiou, and C. Fischione, "Evaluation of localization methods in millimeter-wave wireless systems," in *Proc. IEEE 19th Int. Workshop Computer Aided Modeling and Design of Commun. Links. Netw. (CAMAD)*, Athens, Greece, Dec. 2014, pp. 345–349.
[16] M. Vari and D. Cassioli, "MmWaves RSSI indoor network localization," in *Proc. 2014 IEEE Int. Conf. Commun. Workshops (ICC Workshops)*, Sydney, NSW, Australia, Jun. 2014, pp. 127–132.
[17] A. Fascista, A. Coluccia, H. Wymeersch, and G. Seco-Granados, "Millimeter-wave downlink positioning with a single-antenna receiver," *IEEE Trans. Wireless Commun.*, vol. 18, no. 9, pp. 4479–4490, Sep. 2019.
[18] G. Destino and H. Wymeersch, "On the trade-off between positioning and data rate for mm-wave communication," in *Proc. 2017 IEEE Int. Conf. Commun. Workshops (ICC Workshops)*, Paris, France, May 2017, pp. 797–802.
[19] J. Saloranta and G. Destino, "On the utilization of MIMO-OFDM channel sparsity for accurate positioning," in *Proc. European Sign. Process. Conf.*, Budapest, Hungary, Aug. 2016, pp. 748–752.
[20] N. Garcia, H. Wymeersch, E. G. Larsson, A. M. Haimovich, and M. Coulon, "Direct localization for massive MIMO," *IEEE Trans. Signal Process.*, vol. 65, no. 10, pp. 2475–2487, May 2016.
[21] A. Guerra, F. Guidi, and D. Dardari, "Position and orientation error bound for wideband massive antenna arrays," in *Proc. 2015 IEEE Int. Conf. Commun. Workshops (ICC Workshops)*, London, U.K, Jun. 2015, pp. 853–858.
[22] L. S. Muppirisetty, T. Charalambous, J. Karout, G. Fodor, and H. Wymeersch, "Location-aided pilot contamination avoidance for massive MIMO systems," *IEEE Trans. Wireless Commun.*, vol. 17, no. 4, pp. 2662–2674, Apr. 2018.
[23] A. Shahmansoori, G. E. Garcia, G. Destino, G. Seco-Granados, and H. Wymeersch, "Position and orientation estimation through millimeter wave MIMO in 5G systems," *IEEE Trans. Wireless Commun.*, vol. 17, no. 3, pp. 1822–1835, Mar. 2018.
[24] A. Shahmansoori, G. E. Garcia, G. Destino, G. Seco-Granados, and H. Wymeersch, "5G position and orientation estimation through millimeter wave MIMO," in *Proc. IEEE Glob. Commun. Conf. Workshops (GC Wkshps)*, San Diego, CA, USA, Dec. 2015, pp. 1–6.
[25] Z. Abu-Shaban, X. Zhou, T. Abhayapala, G. Seco-Granados, and H. Wymeersch, "Performance of location and orientation estimation in 5G mmwave systems: Uplink vs downlink," in *Proc. 2018 IEEE Wireless Commun. and Netw. Conf. (WCNC)*, Barcelona, Spain, Apr. 2018, pp. 1–6.
[26] Z. Abu-Shaban, X. Zhou, T. Abhayapala, G. Seco-Granados, and H. Wymeersch, "Error bounds for uplink and downlink 3D localization in 5G mmWave systems," *IEEE Trans. Wireless Commun.*, vol. 17, no. 8, pp. 4939–4954, Aug. 2018.
[27] H. Deng and A. Sayeed, "Mm-wave MIMO channel modeling and user localization using sparse beamspace signatures," in *Proc. IEEE 15th Proc. Int. Workshop Signal Process. Adv. Wireless Commun. (SPAWC)*, Toronto, Canada, Jun. 2014, pp. 130–134.
[28] L. Yin, J. Cao, K. Lin, Z. Deng, and Q. Ni, "A novel positioning-communication integrated signal in wireless communication systems," *IEEE Wireless Commun. Lett.*, vol. 8, no. 5, pp. 1353–1356, Oct. 2019.
[29] J. Ma, C. Liang, C. Xu, and L. Ping, "On orthogonal and superimposed pilot schemes in massive MIMO NOMA systems," *IEEE J. Sel. Areas Commun.*, vol. 35, no. 12, pp. 2696–2707, Dec. 2017.
[30] N. Nonaka, Y. Kishiyama, and K. Higuchi, "Non-orthogonal multiple access using intra-beam superposition coding and SIC in base station cooperative MIMO cellular downlink," in *Proc. IEEE 80th Veh. Technol. Conf. (VTC2014-Fall)*, Vancouver, Canada, Sep. 2014, pp. 1–5.
[31] Y. Saito, Y. Kishiyama, A. Benjebbour, T. Nakamura, A. Li, and K. Higuchi, "Non-orthogonal multiple access (NOMA) for cellular future radio access," in *Proc. IEEE 77th Veh. Technol. Conf. (VTC Spring)*, Dresden, Germany, Jun. 2013, pp. 1–5.
[32] Y. Chen, D. Chen, T. Jiang, and L. Hanzo, "Channel-covariance and angle-of-departure aided hybrid precoding for wideband multiuser millimeter wave MIMO systems," *IEEE Trans. Commun.*, vol. 67, no. 12, pp. 8315–8328, Dec. 2019.
[33] L. Dai, B. Wang, M. Peng, and S. Chen, "Hybrid precoding-based millimeter-wave massive MIMO-NOMA with simultaneous wireless information and power transfer," *IEEE J. Sel. Areas Commun.*, vol. 37, no. 1, pp. 131–141, Jan. 2019.
[34] Y. Chen, D. Chen, T. Jiang, and L. Hanzo, "Millimeter-wave massive MIMO systems relying on generalized sub-array-connected hybrid precoding," *IEEE Trans. Veh. Technol.*, vol. 68, no. 9, pp. 8940–8950, Sep. 2019.
[35] Z. Ding, P. Fan, and H. V. Poor, "Random beamforming in millimeter-wave NOMA networks," *IEEE Access*, vol. 5, pp. 7667–7681, Feb. 2017.
[36] X. Yue, Z. Qin, Y. Liu, S. Kang, and Y. Chen, "A unified framework for non-orthogonal multiple access," *IEEE Trans. Commun.*, vol. 66, no. 11, pp. 5346–5359, Nov. 2018.
[37] S. M. Kay, *Fundamentals of statistical signal processing*. Prentice Hall PTR, 1993.
[38] T. S. Rappaport, S. Shu, R. Mayzus, Z. Hang, Y. Azar, K. Wang, G. N. Wong, J. K. Schulz, M. Samimi, and F. Gutierrez, "Millimeter wave mobile communications for 5G cellular: It will work!" *IEEE Access*, vol. 1, no. 1, pp. 335–349, May 2013.
[39] A. Maltsev, R. Maslennikov, A. Sevastyanov, A. Khoryaev, and A. Lomayev, "Experimental investigations of 60 GHz WLAN systems in office environment," *IEEE J. Sel. Areas Commun.*, vol. 27, no. 8, pp. 1488–1499, Oct. 2009.
[40] C. L. Qian, W. Geng, and T. S. Rappaport, "Channel model for millimeter-wave communications based on geometry statistics," in *Proc. IEEE Glob. Commun. Conf. Workshops (GC Wkshps)*, Austin, TX, USA, Dec. 2014, pp. 427–432.
[41] Q. Li, H. Shirani-Mehr, T. Balercia, A. Papathanassiou, G. Wu, S. Sun, M. K. Samimi, and T. S. Rappaport, "Validation of a geometry-based statistical mmWave channel model using ray-tracing simulation," in *Proc. IEEE 81st Veh. Technol. Conf. (VTC Spring)*, Glasgow, U.K., May 2015, pp. 1–5.

Lincong Han received the B.S. degree in communication engineering from Shandong University (SDU), China, in 2017. She is currently pursuing the Ph.D. degree with the School of Electronic and Information Engineering, Beihang University (BUAA), China. Her current research interests include 5G positioning, wireless communication, non-orthogonal multiple access (NOMA) and Internet of Things networks.

Rongke Liu (SM'19) received the B.S. and Ph.D. degrees from Beihang University in 1996 and 2002, respectively. He was a Visiting Professor with the Florida Institution of Technology, USA, in 2005; The University of Tokyo, Japan, in 2015; and the University of Edinburgh, U.K., in 2018, respectively. He is currently a Full Professor with the School of Electronic and Information Engineering, Beihang University. He received the support of the New Century Excellent Talents Program from the Minister of Education, China. He has attended many special programs, such as China Terrestrial Digital Broadcast Standard. He has published over 100 papers in international conferences and journals. He has been granted 20 patents. His research interest covers wireless multimedia communication, compression coding, channel coding, and aerospace communication.

Zijie Wang received the B.S. degree in electrical and information engineering from Beihang University in 2017. He is currently pursuing the Ph.D. degree with the School of Electronic and Information Engineering, Beihang University, China. His current research interests include global navigation satellite system, terrestrial localization systems, indoor/outdoor seamless positioning, unmanned aerial vehicles, as well as the applications of these technologies to 5G and Internet of Things networks.

Xinwei Yue received the Ph.D. degree in Communication and Information System from Beihang University (BUAA), Beijing, in 2018. He is currently a Associate Professor with the School of Information and Communication Engineering, Beijing Information Science and Technology University (BISTU), Beijing. His research interests include wireless communication (5G), non-orthogonal multiple access (NOMA), physical layer security, cooperative networks and intelligent reflecting surface.

John S. Thompson (F'16) is currently a Professor at the School of Engineering in the University of Edinburgh. He specializes in antenna array processing, cooperative communications systems, energy efficient wireless communications and their applications. He has published in excess of three hundred and fifty papers on these topics. In 2018, he was the co-chair of the IEEE Smartgridcomm conference held in Aalborg, Denmark. He currently participates in two UK research projects which study new concepts for signal processing and for next generation wireless communications. In January 2016, he was elevated to Fellow of the IEEE for contributions to antenna arrays and multi-hop communications. In 2015-2018, he has been recognised by Thomson Reuters as a highly cited researcher.